ADVANCES IN ATMOSPHERIC SCIENCES, VOL. 25, NO. 4, 2008, 632–640

An Updated Coupled Model for Land-Atmosphere Interaction. Part II: Simulations of Biological Processes

ZENG Hongling[1,2,3] (曾红玲), JI Jinjun[4] (季劲钧), and WU Guoxiong[*1] (吴国雄)

[1] *State Key Laboratory of Numerical Modeling for Atmospheric Sciences and Geophysical Fluid Dynamics, Institute of Atmospheric Physics, Chinese Academy of Sciences, Beijing* 100029

[2] *National Climate Center, Beijing* 100081

[3] *Graduate University of Chinese Academy of Sciences, Beijing* 100049

[4] *START Regional Research Center for Temperate East Asia, Institute of Atmospheric Physics, Chinese Academy of Sciences, Beijing* 100029

(Received 16 May 2007; revised 10 December 2007)

ABSTRACT

In Part I, the authors succeeded in coupling the spectral atmospheric model (SAMIL_R42L9) developed at the State Key Laboratory of Numerical Modeling for Atmospheric Sciences and Geophysical Fluid Dynamics, Institute of Atmospheric Physics, Chinese Academy of Sciences (LASG/IAP/CAS) with the land surface model, Atmosphere-Vegetation-Interaction-Model (AVIM) and analyzed the climate basic state and land surface physical fluxes simulated by R42_AVIM. In this Part II, we further evaluate the simulated results of the biological processes, including leaf area index (LAI), biomass and net primary productivity (NPP) etc. Results indicate that R42_AVIM can simulate the global distribution of LAI and has good consistency with the monthly mean LAI provided by Max Planck Institute for Meteorology. The simulated biomass corresponds reasonably to the vegetation classifications. In addition, the simulated annual mean NPP has a consistent distribution with the data provided by IGBP and MODIS, and compares well with the work in literature. This land-atmosphere coupled model will offer a new experiment tool for the research on the two-way interaction between climate and biosphere, and the global terrestrial ecosystem carbon cycle.

Key words: SAMIL-R42L9, R42_AVIM, vegetation-atmosphere interaction

DOI: 10.1007/s00376-008-0632-1

1. Introduction

During the past 20 years, the interaction between the ecosystem and atmosphere has been one of the hot topics in climate change study. Vegetation and climate are always in a dynamical balance. Climate change can have an impact on vegetation and meanwhile, once the vegetation has an obvious change, the climate will be affected too, thus achieving a new balance. Vegetation variation can alter the surface parameters such as albedo, roughness length, zero level displacement etc, then in turn affect regional climate by changing the budgets of water and energy between land and atmosphere. Zheng et al. (2002) found that changes of vegetation exert an important influence on land-air energy equilibrium. Following the change in vegetation, surface released effective thermal fluxes (sensible and latent heat) and Bowen ratio are also changed, which alters the distribution of moist static energy, atmospheric stratification and vertical motion, finally leading to rainfall variation. Vegetation changes over large scales will have important impacts on climate. Many scientists have examined the climatology impacts of Sahara desertification (Charney, 1975; Carson and Sangster, 1981; Laval and Picon, 1986; Sud and Molod, 1988; Xue and Shukla, 1993; Dirmeyer and Shukla, 1996; Zheng and Eltahir, 1997, 1998; Clark et al., 2001) and Amazonian tropical rainforest defor-

*Corresponding author: WU Guoxiong, gxwu@lasg.iap.ac.cn

estation (Henderson-Sellers and Gornitz, 1984; Dickinson and Henderson-Sellers, 1988; Lean and Warrilow, 1989; Nobre et al., 1991; Zeng, 1996). Zeng et al. (1999) found that vegetation's feedback can enhance the interdecadal climate variability in the Sahel. Study on vegetation cover or land-use shows that different vegetation cover or land-use will form different climate and atmosphere circulation. In addition, this impact is comparative to those by other forcing factors like changes in CO_2 concentration, solar radiation etc. (Bonan, 1997; Brovkin et al., 1999; Chase et al., 2000; Fu, 2003). Changes in vegetation also have effects on monsoon. Zheng and Eltahir (1998) indicated that the West Africa monsoon and the corresponding precipitation rely on the location and distribution of vegetation disturbance. Xue et al. (2004, 2006) studied the impacts of land surface processes on the monsoon in East Asia, West Africa and South America, indicating that the exchange of water and energy between vegetation and atmosphere has an important effect on monsoon's development. Li and Xue (2005) studied the impacts of vegetation index on the interannual variation of summer precipitation in the Yellow River basin and indicated that better representation of the vegetation index and its interannual variation may be important for climate prediction.

All these studies indicate that vegetation-atmosphere coupled model is an important tool for research. However, most models used in the above studies are one-sided, that is, using prescribed change of land surface parameters such as vegetation classification, leaf area index (LAI) and vegetation cover etc. to study the response of climate, and ignoring the interaction and feedbacks between them. This cannot satisfy the need for studying the interaction between climate and ecosystem. In recent years, some models began considering the two-way coupling of the vegetation and atmosphere (Foley et al., 1998; Cox, 2001; Lu et al., 2001; Tsvetsinskaya et al., 2001; Dan et al., 2005). However, this kind of work is still Preliminary and most models have relatively low horizontal resolutions. In our work, we have successfully coupled a higher resolution spectral atmospheric model (SAMIL_R42L9) with a land surface process model, Atmosphere-Vegetation-Interaction-Model (AVIM), and analyzed the simulated climate basic state and land surface physical fluxes (Zeng et al., 2008). In this Part II, we further evaluate the simulated biological processes, aiming at offering an experiment tool for future climate-ecosystem interaction study. It is organized as follows: section 2 introduces the data used in this work; section 3 demonstrates the simulated results and makes comparisons with observation. In the last part, the conclusions and discussions are given.

2. Data

In this coupled model, terrestrial ecosystems are classified into 13 types. They are tropical rainforest, broad leaf deciduous trees, broad leaf and needle leaf trees, needle leaf evergreen trees, needle leaf deciduous trees, broadleaf trees with ground cover, ground cover only, broadleaf shrub with ground cover, broadleaf shrubs with bare soil, dwarf trees with ground cover, bare soil, crops, ice etc. (Xue et al., 2004). Figure 1 shows the global distribution of vegetation types. Soil texture is classified as 6 types, such as coarse, medium/coarse, medium, fine/medium, fine, organic etc. (Zobler, 1986).

In order to evaluate the simulated biological processes, we use the following observational data: (1) monthly mean global $0.5^\circ \times 0.5^\circ$ LAI provided by Max Planck Institute for Meteorology (Hagemann, 2002), (2) the International Geosphere Biosphere Programme (IGBP) Global NPP Model Intercomparison Data with the resolution of $0.5^\circ \times 0.5^\circ$ (Cramer et al., 1999), and (3) global annual mean $0.5^\circ \times 0.5^\circ$ MODIS NPP data averaged during 2000–2003 (Zhao et al., 2006).

3. Results

Before analyzing the simulated results, we first introduce the biological process in AVIM. In Part I, we have pointed out that AVIM includes both physical process and biological process and the two components are interactive and have feedbacks on each other. In the plant growth physiological model, photosynthesis, respiration (including growth respiration and maintenance respiration), dry matter allocation in the tissues and decomposition of organic matter are taken into consideration. Net primary productivity can be written as:

$$\mathrm{NPP} = A_\mathrm{c} - R_\mathrm{m} - R_\mathrm{g} \,, \tag{1}$$

where NPP is net primary productivity, A_c is photosynthesis rate, R_m is maintenance respiration rate, R_g is growth respiration rate. Photosynthate (dry matter) can be allocated among the tissues following a definite rule. The variation of biomass of tissues can be expressed as:

$$\frac{dM_i}{dt} = \alpha_i (A_\mathrm{c} - \sum_{i=\mathrm{f,s,r}} \gamma_i M_i) - \beta_i M_i - F_i \,, \tag{2}$$

where M_i is the biomass of leaf, stem or root, α_i is related to the allocation coefficients of dry matter and growth respiration. The subscripts f, s and r denote

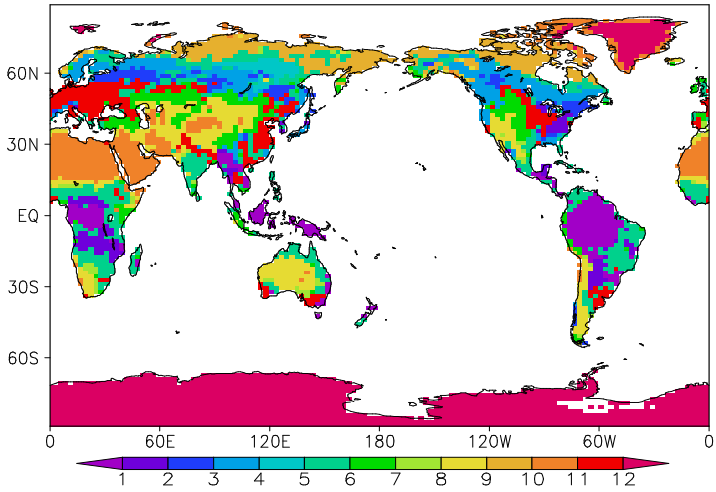

Fig. 1. Vegetation classification in R42_AVIM, There are in turn tropical rainforest, broad leaf deciduous trees, broad leaf and needle leaf trees, needle leaf evergreen trees, needle leaf deciduous trees, broadleaf trees with ground cover, ground cover only, broadleaf shrub with ground cover, broadleaf shrubs with bare soil, dwarf trees with ground cover, bare soil, crops and ice etc.

the variables related to foliage, stem and root, respectively. γ_i and β_i are coefficients of maintenance respiration and falling. F_i represents the disturbances of vegetation biomass, such as fires, plant diseases, herbivory and insect pests. LAI is an important vegetation morphological parameter and its variation can be expressed as:

$$\frac{d\mathrm{LAI}}{dt} = \frac{1}{\rho_\mathrm{f}} \frac{dM_\mathrm{f}}{dt} , \tag{3}$$

where ρ_f is the leaf area for a unit leaf biomass, M_f is leaf biomass. The falling of foliage depends on climatic variations and plant phonological phases.

In AVIM, all these physiological processes are affected by photosynthetic active radiation, CO_2 concentration in the atmosphere, temperature and moisture of the air and soil, which are predicted by the physical process. Meanwhile, the leaf area index, and then the roughness, albedo and other dynamical parameters of vegetation changing with the growth of plants will influence energy, water and CO_2 exchanges between the surface and the atmosphere to realize the interaction between climate and vegetation.

In this article, we run R42_AVIM for 15 years and the means calculated from the last 10 years are taken as the climate base state. In the following, we will analyze the simulated biological processes, including LAI, biomass, NPP etc.

3.1 *LAI*

LAI, an important vegetation morphological parameter, is the projection of total canopy area on a unit land surface area (m^2 m^{-2}). LAI is directly associated with the intensity and allocation of the energy, water, momentum, CO_2 concentration etc. in the canopy. In our work, by comparing with the $0.5° \times 0.5°$ monthly mean LAI data provided by Max Planck Institute for Meteorology, the simulated LAI by R42_AVIM is analyzed.

3.1.1 *Zonally averaged features*

The zonal mean LAI derived from R42_AVIM and Max Planck Institute for Meteorology in January and July are shown in Fig. 2. In January (Fig. 2a), the maximum LAI is centralized in the tropics between 10°S and 10°N with the second maximum between 30°S and 40°S. Except for the regions where needle leaf evergreen trees are distributed, LAI is very low in middle and high latitudes of the northern hemisphere. Compared with the observation, R42_AVIM can basically reproduce the zonal mean feature of LAI. However, biases still exist. The most obvious difference is situated between 20°S and 50°S with a positive bias. This can also be found in the global distribution of LAI (Figs. 3a, c). The regions in the east coast of Australia and southeastern South America have a larger LAI than the observation. The vegetation distribution in these locations needs to be further verified.

In July (Fig. 2b), the maximum LAI is still distributed in tropics. However, LAI in the northern hemisphere shows an obvious seasonal growth, especially in the middle and high latitudes where boreal forests are distributed. Figures 2a and 2b show that the minimum LAI is located between 20° and 30° of

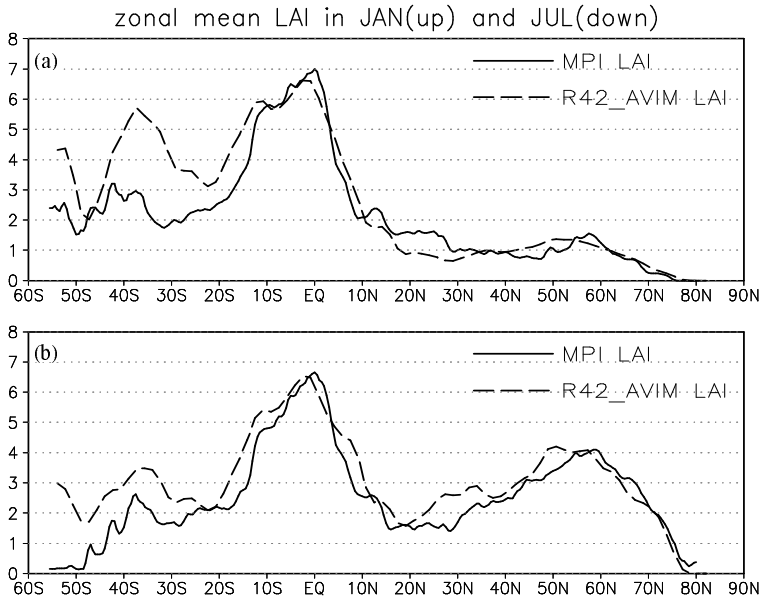

Fig. 2. Zonal mean (a) January, (b) July LAI derived from R42_AVIM and Max Planck Institute for meteorology, units: $m^2\ m^{-2}$.

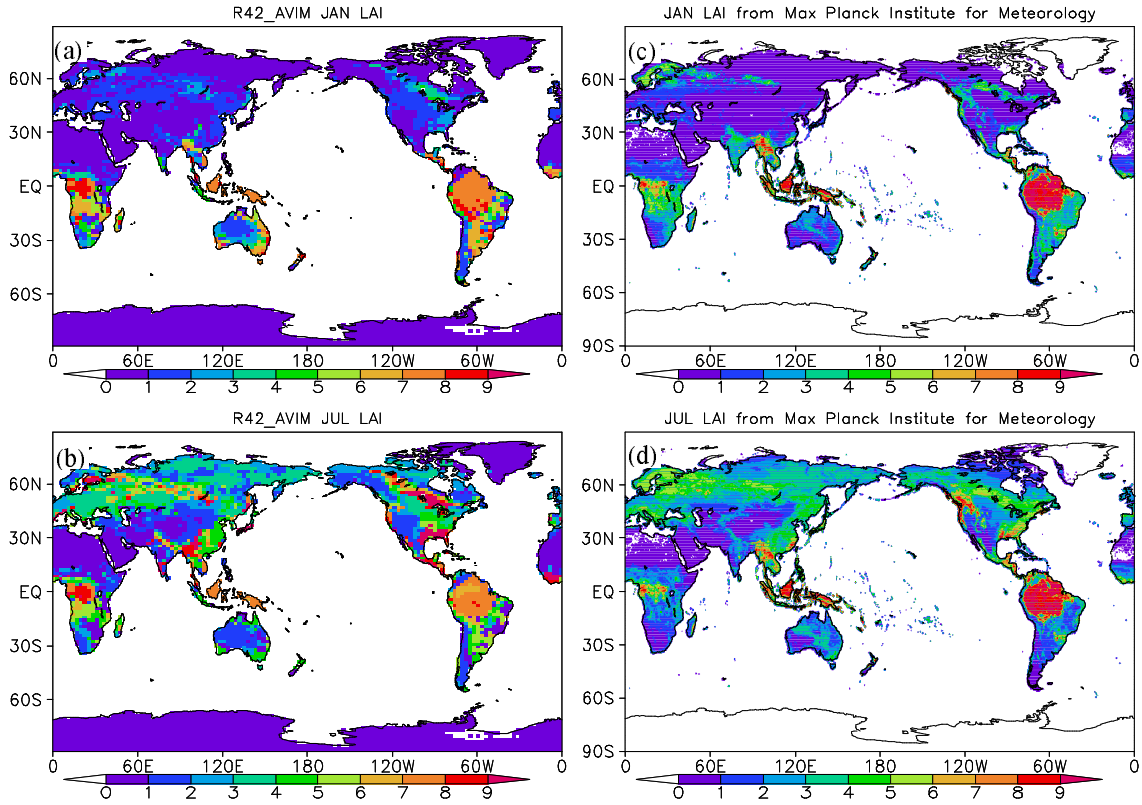

Fig. 3. (a, c) Mean January, (b, d) July LAI derived from (a, b) R42_AVIM and (c, d) Max Planck Institute for meteorology, units: $m^2\ m^{-2}$.

both hemispheres. In those areas, climate is arid with less precipitation, which is not suitable for vegetation growing and most deserts on Earth are distributed there. The simulated LAI is closer to observation in July than that in January. Nevertheless, simulated LAI south of 25°S is a little larger than the observation.

3.1.2 *Global distribution*

Figure 3 shows the global geographical distribution of LAI, including simulated results by R42_AVIM and the observation from Max Planck Institute for Meteorology. In January (Figs. 3a, c), R42_AVIM can reproduce LAI reasonably well, except for the regions where needle leaf evergreen trees are distributed. LAI is very low in middle and high latitudes of the Northern Hemisphere. In the low latitudes such as Indo-China Peninsula, South China and the southeast of America, physical conditions is suitable for vegetation growth and LAI is relatively large. In the southern hemisphere, maximum LAI is mainly distributed in the tropical rainforest of Africa and South America. Compared to observation, there is a negative bias in western Europe, India and western Canada, while a positive bias in middle Africa, southeastern Australia and southeastern South America. In addition, due to the simulated lower surface temperature and less precipitation (shown in Part I), the simulated LAI in tropical rainforest of South America is lower than observation, and needs to be further corrected.

In July, LAI in the northern hemisphere shows an obvious seasonal variation, especially in the middle and high latitudes (Figs. 3b, d). However, the maximum LAI is still distributed in the tropical rainforest. Compared with observation (Fig. 3d), the simulated LAI is larger in the zone near 60°N. Further analysis indicates that this is caused by needle leaf evergreen trees, which have a stronger seasonal growth in JJA in the model simulation. In addition, the larger LAI is just about consistent with the colder zone along 60°N across the Eurasian continent. This shows that larger LAI will cause stronger transpiration and lead to lower surface temperature. The simulated LAI in middle Africa is larger than observation both in January and in July. In addition, in the tropical rainforests of South America, the simulated LAI is also lower than observation, due to the same reason as in January.

3.1.3 *Seasonal variation of LAI for vegetation classifications*

Figure 4 shows the simulated and observed seasonal variations of 11 vegetation types averaged over the northern hemisphere. Figures 4a–k are, in turn, tropical rainforest, broad leaf deciduous trees, broad leaf and needle leaf trees, needle leaf evergreen trees, needle leaf deciduous trees, broadleaf trees with ground cover, ground cover only, broadleaf shrub with ground cover, broadleaf shrubs with bare soil, dwarf trees with ground cover, crops etc. It is clear that R42_AVIM can simulate the seasonal variation of each vegetation type. However, biases still exist. In Fig. 4d, the simulated seasonal variation of needle leaf evergreen trees is too strong. That is, in July and August, the simulated LAI is larger than observation, while smaller from January to June. This can also be seen in the global distribution of LAI in July (Fig. 3b). In addition, for the simulation of broad leaf deciduous trees, broad leaf and needle leaf trees and ground cover only (Figs. 4b, 4c, 4g), although the LAI in January and July is consistent with the observations, the vegetation grows later in spring and languish earlier in autumn. For tropical rainforest (Fig. 4a), the simulated LAI is larger than the observation during all seasons. The simulated LAI of needle leaf deciduous trees is larger in winter and spring, while smaller in summer (Fig. 4e). Broadleaf trees with ground cover have lower LAI in almost all seasons (Fig. 4f), while dwarf trees with ground cover is contrary, having larger LAI in all seasons (Fig. 4j). For crops (Fig. 4k), LAI is a little larger in summer, while a little smaller than the observation in spring and autumn. All of the above indicate that in order to get more reasonable vegetation seasonal variation, the parameters related to phenological phase need further to be corrected.

3.2 *Biomass*

In our work, biomass is the amount of living organism on an unit land area. Figures 5a and 5b show the global distribution of the simulated total biomass and biomass above ground respectively. Biomass above ground is the sum of leaf biomass and stem biomass. Comparing Fig. 5a with Fig. 5b, we can see that in most places, total biomass is close to the biomass above ground, indicating that root biomass is relatively small. However, there is an obvious difference between the two in the regions where grassland or dwarf trees with ground cover are distributed. That is, root biomass is larger in arid or semi-arid areas, which is consistent with the work of Huang et al. (2006). The maximum biomass (12 kg C m^{-2}) is mainly distributed in the tropical rainforests of South America, middle Africa, Indonesia, south China and the Indo-China peninsula. The second maximum of biomass is distributed in boreal forests and the broad leaf deciduous trees of southeastern South America, South Africa, India, southeast of the United States and Australia with a value of about 6–9 kg C m^{-2}. In the deserted area, such as Sahara, Arabia Peninsula and

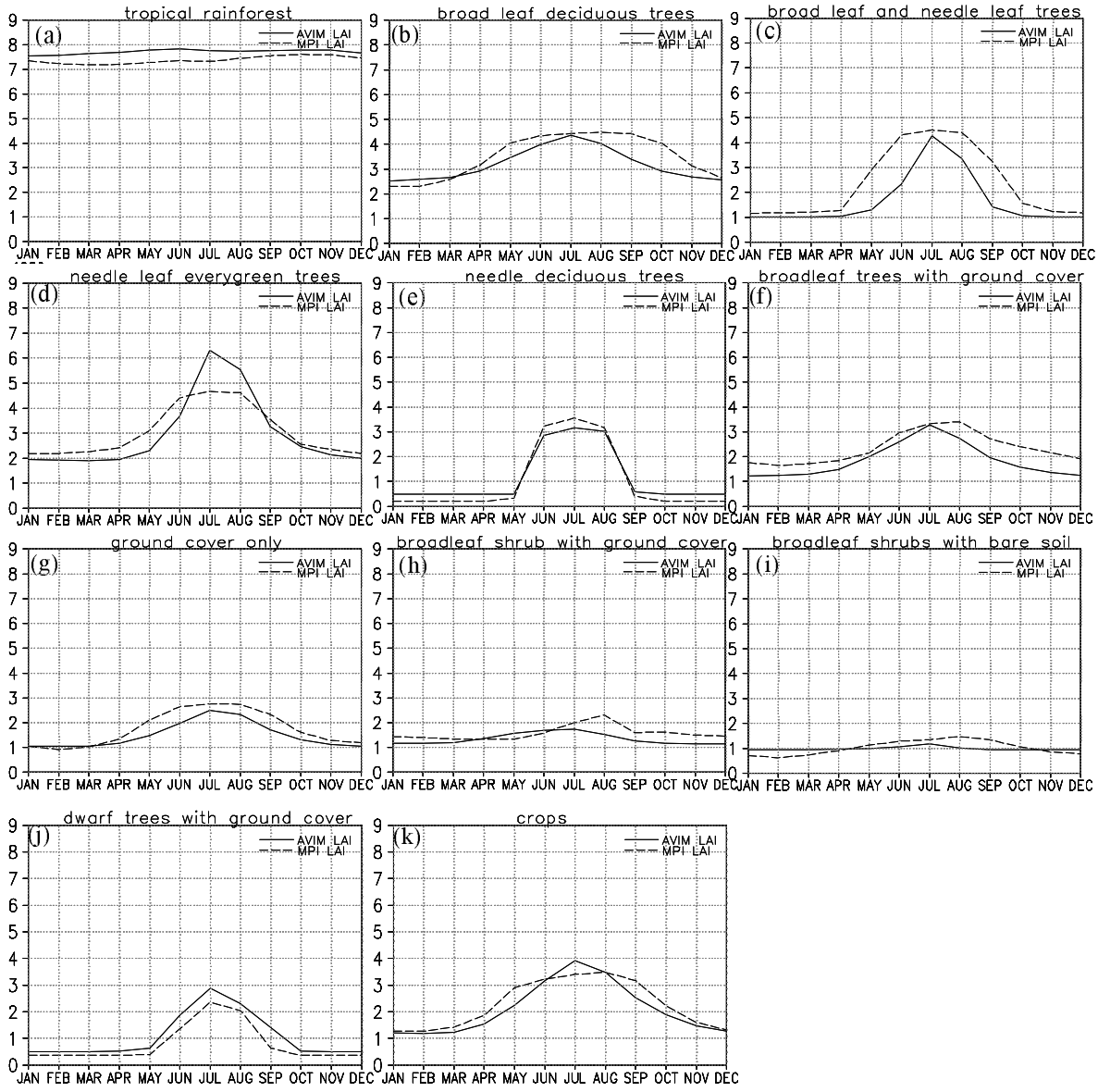

Fig. 4. Seasonal variation of LAI for 11 vegetation classifications in northern hemisphere. (a)–(k) are tropical rainforest, broad leaf deciduous trees, broad leaf and needle leaf trees, needle leaf evergreen trees, needle leaf deciduous trees, broadleaf trees with ground cover, ground cover only, broadleaf shrub with ground cover, broadleaf shrubs with bare soil, dwarf trees with ground cover and crops etc. Units: m^2 m^{-2}.

over the Tibetan Plateau, there is little vegetation and biomass is close to zero. From the simulations in January and July (not shown), total biomass and biomass above ground have relatively weak seasonal variations except for the regions such as East China or the United States of America, where grassland or crops are the dominant vegetation types. Leaf biomass, having similar change as LAI, is the main component causing the seasonal variation of the total biomass.

3.3 *NPP*

Net Primary Productivity (NPP), is defined as the net flux of carbon from the atmosphere into green plants per unit time. NPP is a fundamental ecological variable, not only because it measures the energy input to the biosphere and terrestrial carbon dioxide assimilation, but also because of its significance in indicating the condition of the land surface area and the status of a wide range of ecological processes. On Earth, there are many sorts of ecosystems and their NPP is different from one another. There is a trend of decrease in NPP from tropical rainforests, semitropical evergreen forests, temperate deciduous trees, boreal needle leaf forests, savanna, temperate grassland, tun-

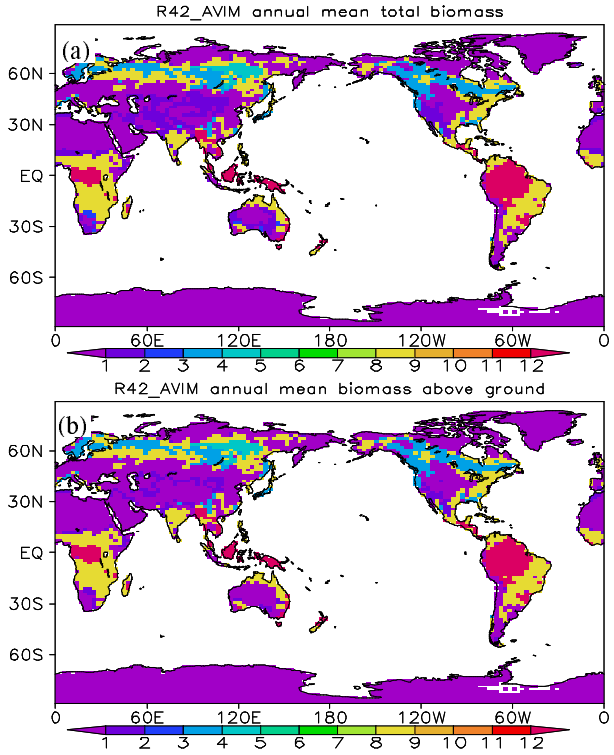

Fig. 5. (a) Annual mean total biomass and (b) biomass above ground derived from R42_AVIM, units: kg C m^{-2}.

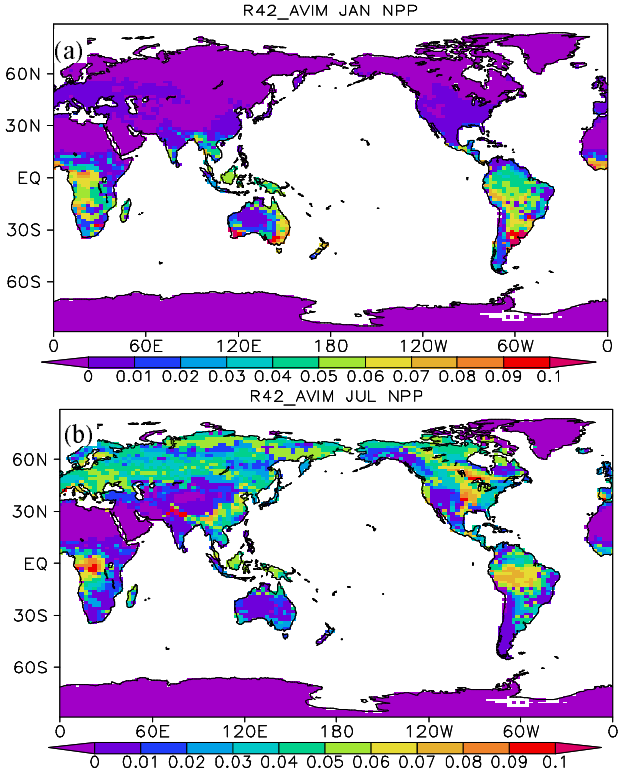

Fig. 6. Mean (a) January and (b) July net primary productivity derived from R42_AVIM, units: kg C m^{-2} mon^{-1}.

dra to deserts. In our work, global distribution of monthly mean and annual mean NPP are analyzed.

3.3.1 *Monthly mean NPP*

Figures 6a and 6b show the simulated global distribution of NPP in January and in July by R42_AVIM. In January, the maximum NPP is mainly distributed in the southern hemisphere, such as the tropical rainforests of South America and Africa, and the broadleaf trees of the east coast of Australia. In the northern hemisphere, the NPP is relatively small except over the Indo-China Peninsula and South China (Fig. 6a). In July, the NPP of the northern hemisphere has an obvious seasonal variation, especially in the boreal forests of middle to high latitudes and crops in East China and southeastern America. However, NPP of the southern hemisphere in July has a northward shift compared to that in January (Fig. 6b).

3.3.2 *Annual Mean NPP*

Figure 7 shows the global distribution of annual mean NPP. The maximum of NPP is mainly distributed in the tropical rainforests, such as in equatorial Africa, Indonesia, Indo-China Peninsula and South America. The second maximum of NPP is in the broadleaf forests of South Africa, east coast of Australia, southeastern South America and Southeast

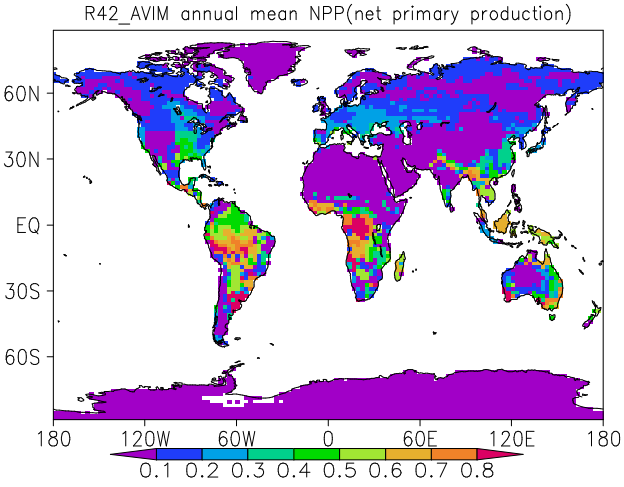

Fig. 7. Annual mean net primary productivity derived from R42_AVIM, units: kg C m^{-2} yr^{-1}.

China. Boreal forests along 50°–60°N have a relatively large NPP distribution too. The simulated global spatial pattern is fairly consistent with the work of Field et al. (1998), indicating that our results are reasonable. However, the simulated NPP by R42_AVIM has

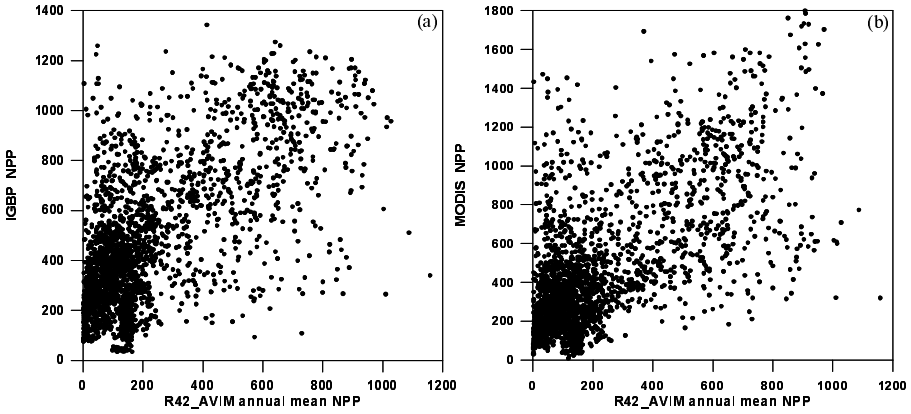

Fig. 8. Scatter plot of annual mean net primary productivity derived from (a) R42_AVIM and IGBP NPP, (b) R42_AVIM and MODIS NPP, units: g C m^{-2} yr^{-1}.

a negative bias of about 0.1 kg C m^{-2} yr^{-1}.

In order to evaluate the simulated NPP on a whole, Fig. 8a and Fig. 8b show the scatter plots of R42_AVIM simulation with annual mean NPP derived from International Geosphere-Biosphere Programme (IGBP) and Moderate-resolution Imaging Spectroradiometer (MODIS) respectively. We can see that the simulated results are more consistent with MODIS NPP than IGBP NPP, and the IGBP NPP is larger than the simulated NPP. However, the simulated NPP has a linear correlation with the above two data.

4. Conclusions

Based on Part I, in Part II, the simulated results of the biological processes including LAI, biomass and NPP are further evaluated. Results show that R42_AVIM can simulate the zonal mean and global geographical distributions of LAI, which is well consistent with the monthly mean LAI provided by Max Planck Institute for Meteorology. The simulated total biomass and biomass above ground are reasonably well corresponding to the vegetation classifications. Moreover, the simulated annual mean NPP distribution is consistent with the data provided by IGBP and MODIS, and similar to the work of Field et al. (1998). All of the results imply that this land-atmosphere coupled model will offer a new experiment platform for the research on interaction between climate and biosphere, and the global terrestrial ecosystem carbon cycle.

Nevertheless, there are some biases. The simulated LAI in South America has a negative bias, which is attributed to the lower simulated temperature and less precipitation there (shown in Part I). Simulated seasonal variation of needle leaf evergreen trees is too strong. Some other vegetation types, such as broad leaf deciduous trees, broad leaf and needle leaf trees and ground cover only, grow later in spring and languish earlier in autumn. So, the simulated LAI seasonal variation needs to be further improved. Due to the deficiency of observations and the complex surface land cover, our work is still preliminary. In order to improve land surface parameters and offer a better experimental platform for climate-ecosystem study, we need to compare our simulations with more observations and multi-model results.

Acknowledgements. This study is jointly supported by the National Key Basic Research 2006CB403607, the Chinese Academy of Sciences (CAS) International Partnership Creative Group "The climate system model development and application studies" and the National Natural Sciences Foundation of China under Grant Nos. 40221503, 40475027 and 40523001.

REFERENCES

Bonan, G. B., 1997: Effects of land use on the climate of the United States. *Climate Change*, **37**, 449–486.

Brovkin, V., A. Ganopolski, M. Claussen, C. Kubatzki, and V. Petoukhov, 1999: Modelling climate response to historical land cover change. *Global Ecology and Biogeography*, **8**(6), 509–517.

Carson, D. J., and A. J. Sangster, 1981: The influence of land-surface albedo and soil moisture on general circulation model simulation. Research activities in atmospheric and oceanic modeling, I. D. Rutherford, Ed., *Numerical Experimentation Program Rept.*, Vol. 2, 5.14–5.21.

Charney, J. G., 1975: Dynamics of deserts and drought in the Sahel. *Quart. J. Roy. Meteor. Soc.*, **101**(428), 193–202.

Chase, T. N., R. A. Pielke Sr., T. G. F. Kittel, R. R. Nemani, and S. W. Running, 2000: Simulated impacts of historical land cover changes on global climate in northern winter. *Climate Dyn.*, **16**, 93–105.

Clark, D. B., Y. K. Xue, R. J. Harding, and P. J. Valdes, 2001: Modeling the impact of land surface degradation on the climate of tropical North Africa. *J.*

Climate, **14**, 1809–1822.

Cox, P. M., 2001: Bringing life and carbon to the GCM land surface processes. *BAHC/GEWEX News Joint Issue*, 10–11.

Cramer, W., and Coauthors, 1999: Comparing global models of terrestrial net primary productivity(NPP): Overview and key results. *Global Change Biology*, **5**(Suppl.1), 1–15.

Dan, L., J. J. Ji, and Y. P. Li, 2005: Climatic and Biological Simulations in a Two-Way Coupled Atmospheric-Biosphere Model (CABM). *Global and Planetary Change*, **47**, 153–169.

Dickinson, R. E., and A. Henderson-Sellers, 1988: Modelling tropical deforestation: A study of GCM land -surface parameterizations. *Quart. J. Roy. Meteor. Soc.*, **114**, 439–462.

Dirmeyer, P. A., and J. Shukla, 1996: The effect on regional and global climate of expansion of the world's deserts. *Quart. J. Roy. Meteor. Soc.*, **122**, 451–482.

Field, C. B., Behrenfeld, M. J., Randersoin, and J. T., Falkowski, P., 1998: Primary production of the biosphere: integrating terrestrial and oceanic components. *Science*, **281**, 237–240

Foley, J. A., S. Levis, I. C. Prentice, D. Pollard, and S. L. Thompson, 1998: Coupling dynamic models of climate and vegetation. *Global Change Biology*, **4**, 561–579.

Fu, C. B., 2003: Potential impacts of human induced land cover change on East Asia monsoon. *Global and Planetary Change*, **37**, 219–229.

Hagemann, S., 2002: An improved land surface parameter dataset for global and regional climate models. Max Planck Inst. Meteorol(MPI) Rept., 336pp.

Henderson-Sellers, A., and V. Gornitz, 1984: Possible climatic impacts of land cover transformations with particular emphasis on tropical deforestation. *Climate Change*, **6**, 231–258.

Huang, M., J. J. Ji, M. K. Cao, and K. R. Li, 2006: Modeling study of vegetation shoot and root biomass in China. *Acta Ecologica Sinica*, **26**(12), 4156–4163.

Laval, K., and L. Picon, 1986: Effect of a change of the surface albedo of the Sahel on climate. *J Atmos. Sci.*, **43**, 2418–2429.

Lean, J., and D. A. Warrilow, 1989: Simulation of the regional climatic impact of Amazon deforestation. *Nature*, **342**, 411–413.

Li, W. P., and Y. K. Xue, 2005: Numerical simulation of the impact of vegetation index on the interannual variation of summer precipitation in the Yellow River Basin. *Adv. Atmos. Sci.*, **22**, 865–876.

Lu, L. X., R. A. Pielke Sr., G. E. Liston, W. Parton, D. Ojima, and M. Hartman, 2001: Implementation of a two-way interactive atmospheric and ecological model and its application to the Central United States. *J. Climate*, **14**, 900–919.

Nobre, C. A., P. J. Sellers, and J. Shukla, 1991: Amazonia deforestation and regional climate change. *J. Climate*, **4**, 957–988.

Sud, Y. C., and A. Molod, 1988: A GCM simulation study of the influence of Saharan evapotranspiration and surface-albedo anomalies on July circulation and rainfall. *Mon. Wea. Rev.*, **116**(11), 2388–2408.

Tsvetsinskaya, E. A., L. O. Mearns, and W. E. Easterling, 2001: Investigating the effect of seasonal plant growth and development in 3-dimensional atmospheric simulations: Part I. Simulations of Surface Fluxes over the Growing Season. *J. Climate*, **14**, 692–709.

Xue, Y., and J. Shukla, 1993: The influence of land surface properties on Sahel climate. Part I: Desertification. *J. Climate*, **6**, 2232–2245.

Xue, Y., H. M. H. Juang, W. P. Li, S. Prince, R. DeFries, Y. Jiao, and R. Vasic, 2004: Role of land surface processes in monsoon development: East Asia and West Africa. *J. Geophys. Res.*, **109**, D03105, doi: 10.1029/2003JD003356.

Xue, Y., F. D. Sales, W. P. Li, C. R. Mechoso, C. A. Nobre, and H. M. Juang, 2006: Role of land surface processes in South American monsoon. *J. Climate*, **19**, 741–762.

Zhao, M. S., S. W. Running, and R. R. Nemani, 2006: Sensitivity of Moderate Resolution Imaging Spectroradiometer (MODIS) terrestrial primary production to the accuracy of meteorological reanalyses. *J. Geophys. Res.*, **111**, G01002, doi: 10.1029/2004JG000004.

Zeng, H. L., Z. Z. Wang, J. J. Ji, and G. X. Wu, 2008: An updated coupled model for land-atmosphere interaction. Part I: Simulations of physical processes. *Adv. Atmos. Sci.*, **25**(4), 619–631, DOI: 10.1007/s00376-008-0619-y.

Zeng, N., 1996: Climate impact of Amazon deforestation—A mechanistic model study. *J. Climate*, **9**, 859–883.

Zeng, N., J. D. Neelin, K. M. Lau, and C. J. Tucker, 1999: Enhancement of interdecadal climate variability in the Sahel by vegetation interaction. *Science*, **286**, 1537–1540.

Zheng, X. Y., and E. A. B. Eltahir, 1997: The response to deforestation and desertificationin a model of West African monsoons. *Geophys. Res. Lett.*, **24**(2), 155–158.

Zheng, X. Y., and E. A. B. Eltahir, 1998: The role of vegetation in the dynamics of West African monsoons. *J. Climate*, **11**(8), 2078–2096.

Zheng, Y. Q., Y. F. Qian, M. Q. Miao, G. Yu, D. H. Zhang, and Y. S. Kong, 2002: The effects of vegetation change on regional climate II: Mechanisms. *Acta Meteorologica Sinica*, **60**, 17–30. (in Chinese)

Zobler, L., 1986: A world soil file for global climate modeling. NASA Tech. Memo. 87802, NASA Goddard Institute for Space Studies, New York, U. S. A., 33pp.